Nuclear jets in heavy-ion collisions

P. Napolitani, M. Colonna

Version of Record: https://www.sciencedirect.com/science/article/pii/S0370269319305477
Manuscript_8239c6b2edbbfaa338e7f55977e288ea

Nuclear jets in heavy-ion collisions

P. Napolitani[a], M. Colonna[b]

[a]IPN, CNRS/IN2P3, Université Paris-Sud 11, Université Paris-Saclay, 91406 Orsay Cedex, France
[b]INFN-LNS, Laboratori Nazionali del Sud, 95123 Catania, Italy

Abstract

Head-on collisions between nuclei of different size at Fermi energies may give rise to extremely deformed dynamical regimes and patterns. Those latter, may suddenly turn into a stream of nuclear clusters, resembling collimated jets. This mechanism, which could be easily addressed in experiments, is simulated in the framework of stochastic one-body approaches. We employ the Boltzmann-Langevin equation to specifically address out-of-equilibrium conditions and handle dynamical fluctuations. An interesting interplay between surface and volume instabilities is discussed for the first time, leading to the appearing of stable and rather regular patterns of streaming clusters.

1. Introduction

From microphysics to cosmological scale, jet regimes are frequent. They are collimated streams of matter which eventually clusterise into packets, yielding a variety of nonlinear behaviours [1, 2, 3]. Since early nuclear-fission models [4, 5, 6], the occurrence and rupture of deformed stretched structures in nuclear reactions, like neck configurations, suggested the analogy to viscous liquids subject to the Rayleigh instability [7, 8, 9], whereby a fluid thread breaks up into droplets. Such analogy became emblematic [10, 11, 12] in explaining nuclear reactions from low-energy to Fermi energy (i.e. above about 30 MeV per nucleon). We explore the possibility that, beyond Fermi energy, columnar configurations could arise in heavy-ion collisions from different conditions than those producing a neck in dinuclear systems [13, 14], and that they undergo rupture from mechanisms other than Rayleigh-type instabilities, i.e. from mechanisms that are almost unrelated to cohesive properties. In analogy with columnar streams of matter which are widely encountered in nature, from liquid to granular flows, we may generally refer to these configurations as nuclear jets. By employing a theoretical approach where we add collisional correlations and Langevin-type fluctuations to a mean-field description, we found that nuclear jets are frequent in collisions of nuclei of asymmetric size around Fermi energy. From the analysis of the type of instability which triggers rupture, we advance the conclusion that the clusterisation of the jet reflects an interesting interplay between volume and surface instabilities, with a leading role played by nucleon-nucleon (N-N) correlations and volume instabilities. More specifically, we find that clusterisation along the jet selects small sizes, favouring light nuclear clusters. This may lead to a new production mechanism of exotic clusters.

2. Modelling nuclear jets

Widely used in many branches of physics, microscopic theories of transport phenomena are applied to heavy-ion collisions in a broad range of energies. For instance, nuclear transport dynamics can be put in the form of a kinetic equation where the propagation of the one-body density f in phase-space depends upon the effective Hamiltonian $h[f]$ and the contribution of N-N collisional correlations. To describe nuclear jets we should explain how clusterisation progresses in colliding nuclei. Such a chaotic mechanism could be handled by stochastic transport theories [15] as those applied to diffusive processes, like the Brownian motion [16]. The additional degrees of freedom involved in turning the jet into a stream of clusters can be introduced in approximate form by the action of a fluctuating seed on the one-body density, so that a single mean-field path f taken at a given time, splits into a subensemble of new trajectories $f^{(n)}$ which propagate at subsequent times. Such scheme is represented by the Boltzmann-Langevin equation [17, 18]

$$\frac{\partial f^{(n)}}{\partial t} = \{h[f^{(n)}], f^{(n)}\} + \bar{I}_{\rm coll}[f^{(n)}] + \delta I_{\rm coll}[f^{(n)}] \,, \qquad (1)$$

where the Langevin term $\delta I_{\rm coll}[f^{(n)}]$ acts as a fluctuating contribution around the average collision term $\bar{I}_{\rm coll}[f^{(n)}]$, in the spirit of the Brownian motion. The Langevin term leads to a diffusion coefficient $\mathcal{D}_{\rm coll}$; it can produce bifurcations, and generates fluctuations intermittently in time.

Clusterisation is a general catastrophic process characterising Fermi liquids [19], stemming from conditions of instability and fluctuations. As a response, a combination of several fluctuation modes of large-amplitude are induced, where neutrons and protons may oscillate in phase or out of phase. In this process, the most amplified wavelengths are reflected into density ripples and, finally, into fragment formation. Their sizes has been found to characterise small atomic nuclei [20, 21, 22]. From the out-of-phase oscillations of neutrons and protons another process, isospin distillation, arises in relation to the nu-

clear symmetry energy, which leads to more isosymmetric fragments, thus affecting the final isotopic distributions of reaction products [14, 23]. Clusterisation can be efficiently handled by Eq. (1). We introduced the Boltzmann Langevin One Body (BLOB) approach [24, 25] as a corresponding numerical realisation in three dimensions. At variance with earlier approaches, like the Brownian One-Body (BOB) model, where fluctuations were induced by a stochastic force term acting once volume instabilities appear [16, 26], the BLOB approach implements the stochastic collision integral of Eq.(1), all along the reaction path, allowing a more accurate description of the reaction dynamics. In particular, both isoscalar and isovector mechanisms (i.e. fragment formation and distillation) are satisfactorily handled with BLOB in nuclear matter [25]. We employ this approach to gain insight into the jet mechanism, and the underlying instability. For comparison, we also employ an approximate version of stochastic mean field [27], where we suppress both N-N collisions and related fluctuations in the residual contribution of Eq. (1) and replace them by simple coarse-grained effects related to the mean field implementation $\bar{I}_{\rm coll} + \delta I_{\rm coll} \rightarrow \delta I_{\rm noise}$. This collisionless approach is still able to activate breakup mechanisms but, relative to the BLOB approach, it leads to a drastically reduced effective diffusion coefficient $\mathcal{D}_{\rm noise} \ll \mathcal{D}_{\rm coll}$. See Appendix A for simulation parameters.

3. Results

When atomic nuclei of different size are involved in head-on collisions above Fermi energy, the heaviest nucleus is heated up by the collision without suffering drastic modifications and it produces the heavier residue in the exit channel: we name it A_1. Contrarily, the lighter partner tends to disintegrate into a jet of fast-streaming low-density matter, producing the second, third, etc. largest fragments, named A_2, A_3, etc., respectively. This is the pattern which has been reported in experiments, e.g. in ref. [28], and which is also observed in BLOB simulations. As a specific example, we analyse hereafter a typical system where the jet process should occur. A calculation illustrated in Fig. 1 tracks the evolution of the density distribution in configuration space in the asymmetric system ^{36}Ar+^{58}Ni at 74 A MeV (head-on collisions) and in the corresponding symmetric systems ^{36}Ar+^{36}Ar and ^{58}Ni+^{58}Ni for single stochastic events, chosen among the most probable ones. Only head-on collisions are selected by letting the impact parameter b vary uniformly from 0 to 1 fm. While the symmetric channels in Fig. 1(d) and 1(e) manifest significant radial expansion, which is the well known signature of multifragmentation and vaporisation mechanisms [29, 30], the asymmetric channels in Fig.1(a) exhibit a columnar jet formation in the forward sector relative to A_1. Since early times, the jet experiences a density drop along the longitudinal axis within 1/3 to 1/8 of the nuclear saturation density $\rho_{\rm sat}$, as shown in Fig. 1(c). The collisionless approach, Fig. 1(b) leads to a neck-like pattern instead, where one or few small fragments are situated at intermediate rapidity relative to two larger fragments.

A survey of the most frequent configurations of forward fragment emission in ^{36}Ar+^{58}Ni is presented in Fig. 2 as a function of the incident energy. In Fig. 2(a), jets from BLOB calculations arise above 40AMeV and dominate the exit channel from 52 to 74AMeV, while at lower energy binary and neck-like mechanisms gain larger share. At larger bombarding energy jets expand in elongation and width, displaying a more turbulent pattern. Fig. 2(b) tracks the multiplicity of intermediate-mass fragments (IMF) according to two selections labelled IMF$_1$ when accounting for any fragment other than free nucleons and protons, and IMF$_2$ when deuterons, tritons, 3He and α particles are additionally excluded. At variance with the collisionless approach, the BLOB simulation yields different populations IMF$_1$ and IMF$_2$. The larger growth time and earlier saturation of the population IMF$_2$ relative to IMF$_1$ as a function of the incident energy, indicates that the production of light charged particles (LCP) contributes largely to the IMF multiplicity, involving more and more mass from the target-like nucleus.

There is actually a fundamental difference between neck fragments and IMF arising along a jet, as examined in Fig. 3 for the system at 74 AMeV. Relying either on BLOB or on the collisionless version, Fig. 3(a) traces the time evolution of the average multiplicity of fragments where A_1 is excluded, selecting either the population IMF$_1$ or IMF$_2$. Right after maximum dilution is reached in the system at the time $t_{\rm md}$, the sudden growth of multiplicity signals either the re-separation of projectile and

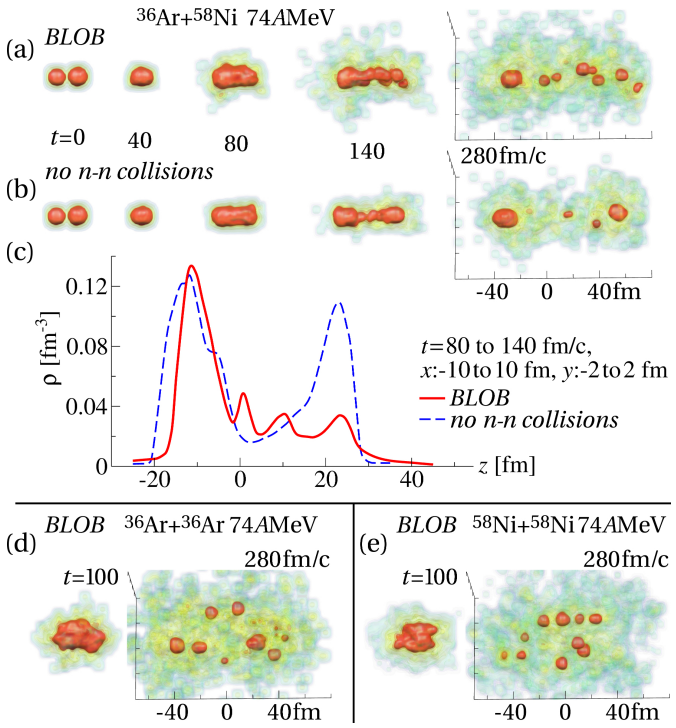

Figure 1: Simulation of ^{36}Ar+^{58}Ni at 74 A MeV with BLOB (a) and the collisionless approach (b), for one single event. (c), Corresponding density profile evaluated around the collision axis z (cell size: 20fm in impact-parameter direction x and 4fm in out-of-reaction-plane direction y) and averaged in a time span from 80 to 140fm/c. (d,e), BLOB simulations of ^{36}Ar+^{36}Ar and ^{58}Ni+^{58}Ni at 74 A MeV.

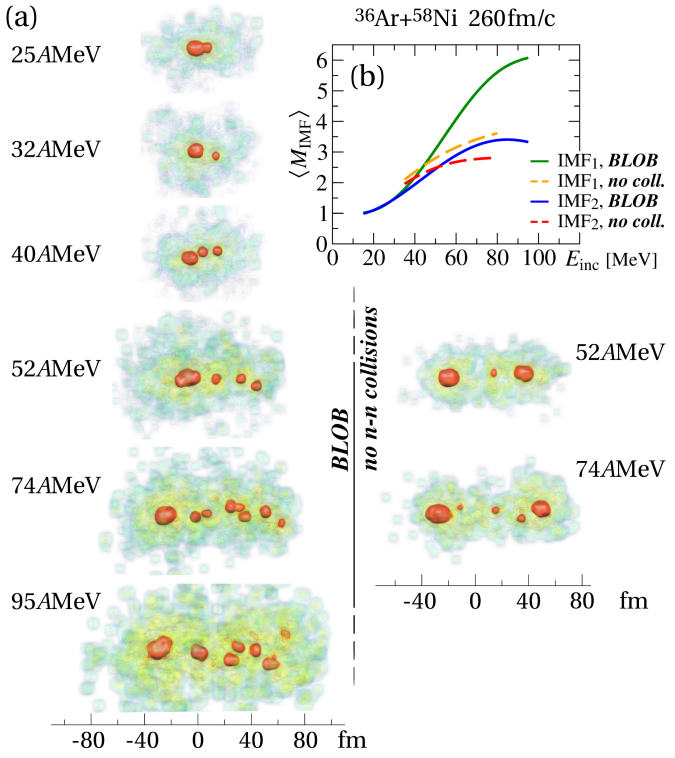

Figure 2: (a) Single events simulated with BLOB and the collisionless approach for ^{36}Ar+^{58}Ni at 260fm/c as a function of bombarding energy; the event at 74 *A*MeV was presented in its full time evolution in Figs. 1(a) and 1(b). See supplementary material for movies tracking the time evolution of events at 40, 52, 74 and 95 *A*MeV. (b) average multiplicity of fragments. n and p are excluded in the selection IMF$_1$. n,p,d,t,^{3}He,α are excluded in the selection IMF$_2$.

target or the development of the jet. At later times, in the collisionless approach the further evolution of multiplicity is slow and reflects a chiefly binary split with the possible presence of one or more light fragments. On the other hand, the BLOB calculation suggests that the multiplicity continues to grow until around 280 fm/c due to the production of LCP. From this evolution, we can associate the beginning of instability growth, discussed in the following, to the time interval ranging from 110 to 120 fm/c. The mass of the fragments A_1, A_2, A_3, etc. is analysed in Fig. 3(b) as a function of the longitudinal velocity v_z (along the beam axis) for events where at least three fragments are produced. In the collisionless approach we found that A_2 is characterised by the largest forward velocity, followed by smaller fragments, recalling the physics of peripheral or semi-central collisions [31, 32], where cohesive properties, related to nuclear surface tension, have usually been invoked to explain the formation of clusters. On the contrary, the BLOB calculation suggests a reverse hierarchy, where larger longitudinal velocities tend to be correlated to smaller sizes; the same picture can be drawn from the density profile in Fig. 1(c), where a series of maxima correspond to inhomogeneities and nesting places for clusters along a jet. Such behaviour is typically related to volume instability, and not to cohesive properties. The drop to low density also triggers the occurrence of isospin effects [21, 33, 34, 35, 36] both in the jet formation and in the neck mechanism. The average isotopic composition $<N/Z>$ of A_1, A_2 and of the lighter fragments (A_3...) is tracked in Fig. 3(c) for events where at least three fragments are formed. In the collisionless approach, lighter fragments (A_3...) exhibit a larger average neutron-to-proton ratio than A_1 and A_2, as expected for a migration process towards the low-density neck [37, 33, 38]. On the other hand, in the BLOB approach, the A_2 fragments are more neutron rich than the system and the other lighter fragments reach even higher values. This results from the combination of two effects: an intense prompt emission of protons and α enhances the neutron excess of the rest of the system; at the same time, this latter undergoes isospin distillation so that the most volatile phase gains additional neutron excess. Such behaviour, determined by isovector fluctuations [23, 39], is one more indication that the jet should involve volume instabilities. Fig. 4 shows the results obtained after considering the de-excitation of primary fragments. The analysis is extended also to less central impact parameters. One can observe that, despite the decay of the heavy remnant (whose excitation energy is close to 3 MeV per nucleon), the jet features discussed

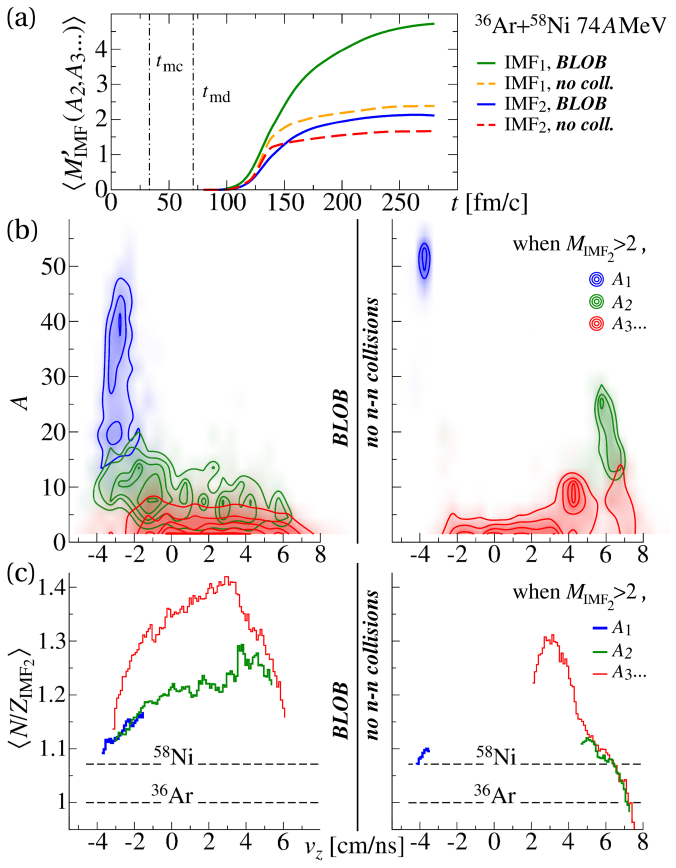

Figure 3: In ^{36}Ar+^{58}Ni at 74 *A*MeV. (a) Time evolution of the average multiplicity of fragments of smaller size than A_1. Times t = 0, t_{mc} (maximum compression) and t_{md} (maximum dilution) are indicated. Selections IMF$_1$ and IMF$_2$ are defined as in Fig. 2(b). (b) Correlation between fragment mass and longitudinal velocity v_z at t_{stop}, for the distribution of A_1, A_2, and the remaining lighter fragments (A_3...) in events where at least three fragments belonging to IMF$_2$ are observed. (c) Isotopic content averaged over IMF$_2$ as a function of v_z at t_{stop}. Same selections as in (b).

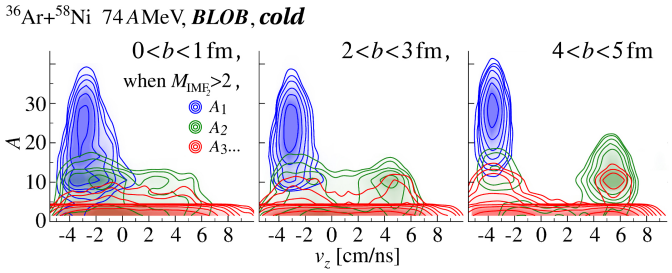

Figure 4: Like in Fig. 3(b) for the cold system and three intervals of the impact parameter b.

above are still quite evident. Indeed, the low excitation energy (peaked around 2 MeV per nucleon) and the large momentum of the jet fragments preserve their original dynamical signature. Moreover, it can be seen that the jet pattern persists up to larger impact parameters, being lost, for the cold residues, for b larger than 4 fm, where two heavy remnants appear.

4. Discussion: surface instability or volume instability?

From the above analysis, two types of instabilities emerge as possible contributions to clusterisation, according to whether they prevalently involve the surface or the volume of the jet. To explore their mutual role, fig. 5(a) tracks the density of emerging ripples of the mean-field potential, $\rho_{\rm well}$, in the jet region as a function of time, calculated with BLOB for the system ^{36}Ar+^{58}Ni at 74 AMeV. From a 3D analysis of the potential slope, $\rho_{\rm well}$ is the mean density measured in a potential concavity as it stands out of the background. When averaging over several events, we find that $\langle\rho_{\rm well}\rangle$ suddenly drops below a fourth of $\rho_{\rm sat}$. Later on, these ripples may separate into fragments of mass A, relax in shape and thermalise, so that it is possible to extract the temperature T and the mean density $\rho_{\rm frag}$ of the fragment measured in the corresponding potential well. By averaging over several events, Fig. 5(b) investigates the correlation between these two quantities; IMF with $A > 4$ are formed at temperatures $\langle T\rangle$ around 3 MeV in a wide density region, from $\rho_{\rm sat}/2$ to $\rho_{\rm sat}/4$, while lighter clusters (d, t, ^{3}He, α) are produced at smaller temperatures in density tails below $\rho_{\rm sat}/5$. While the significantly deformed columnar-like configuration may suggest a Plateau-Rayleigh surface instability, these density and temperature conditions are compatible with a volume instability of spinodal type. Fig. 5(c) compares analytic expectations for both instabilities at different densities, and for a temperature of 3 MeV, consistent with the production of IMF with $A > 4$. In nuclear reactions, the Plateau-Rayleigh instability is commonly envisaged in nuclear fission or in the breakup of a neck. A schematic dispersion relation, see dashed lines in Fig. 5(c), relates the growth rate for an unstable mode of wavenumber k to the surface tension γ and to the geometric properties of a columnar configuration of radius r as [8]

$$(\Gamma_{k,\rm surf})^2 = \frac{\gamma}{\rho m r^3}\frac{I_1(kr)}{I_0(kr)}kr(1-k^2r^2)\,, \qquad (2)$$

where I_0 and I_1 are modified Bessel functions and m is the nucleon mass. The jet is approximated to a cylinder of length $l_{\rm jet}$ containing a stream of clusters of mass A_i which travel in forward direction and which do not include the heavy residue A_1. Further restrictions select only jets containing at least three clusters. The local density ρ is averaged over the jet volume, and the radius r is promptly obtained as a function of ρ. We consider $r \approx 2$ fm, which corresponds to the configurations obtained in the numerical simulations. The expression of the surface tension γ should take into account the low local density ρ, as well as the charge asymmetry $\beta = (\rho_n - \rho_p)/\rho$ of the emerging fragments (Fig. 3) and the finite temperature T (see Appendix A). The volume instability applies primarily to regions of the equation of state where nuclear compressibility is negative (pressure reducing with increasing density), resulting in instabilities of spinodal type [40, 21]. It has been widely investigated in nuclear systems at low density which disintegrate in several similar-size fragments [22]. In nuclear matter [41, 42, 25], within the linear-response approximation, the dispersion relation, see solid lines in Fig. 5(c), is

$$1 + \frac{1}{\tilde{F}_0(k,T)} = \frac{\Gamma_{k,\rm vol}}{kv_{\rm F}}\arctan\left(\frac{kv_{\rm F}}{\Gamma_{k,\rm vol}}\right)\,, \qquad (3)$$

where $v_{\rm F}$ is the Fermi velocity and $\tilde{F}_0(k,T) = (\mu(T)/\epsilon_{\rm F})F_0g(k)$ is the effective Landau parameter including a dependence on temperature, through the chemical potential $\mu(T)$, the Fermi en-

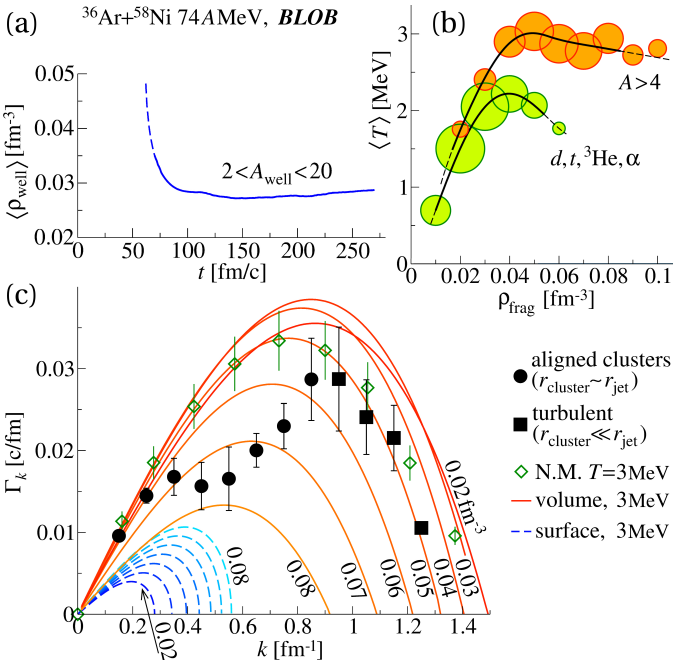

Figure 5: In ^{36}Ar+^{58}Ni at 74 AMeV. (a) Time evolution of the density $\langle\rho_{\rm well}\rangle$ of density ripples associated with nesting fragments of size $A_{\rm well}$. (b) Correlation between temperature and density for light clusters (d, t, ^{3}He, α) and remaining IMFs ($A > 4$) found in the jet ($A1$ is excluded) in a time range from 150 to 280 fm/c; symbol areas are normalised to total production yields. (c) Growth rate as a function of the k number for two jet splitting geometries (see text); error bars are related to the initial time defining the onset of instabilities, ranging from 110 to 120 fm/c. For comparison, analytic dispersion relations at T = 3MeV and at different densities for volume (i.e. spinodal) and surface (i.e. Plateau-Rayleigh) instabilities are shown. BLOB calculations in nuclear matter (N.M.) at $\rho_{\rm sat}/3$ and T = 3MeV, from ref. [25], are also shown.

ergy ϵ_F, and the range of the nuclear interaction via the term $g(k)$; the range dependence (see Appendix A) imposes an ultraviolet cutoff which bends the dispersion relation back to zero at small wavelengths (or large k), see Fig.5. A BLOB calculation of the spinodal instability in initially homogeneous nuclear matter at $\rho_{sat}/3$ and 3 MeV is added for comparison (from ref. [25]). In this case a Fourier analysis of the spatial density fluctuations was performed, thus allowing to evaluate the fluctuation variance associated with a given wave number k. The early time evolution of the latter quantity exhibits an exponential increase and the corresponding growth rate is reported in Fig.5 as a function of k (open diamonds).

We compared the above analytic prescriptions to numerical results obtained with BLOB for the jet mechanism in ^{36}Ar+^{58}Ni at 74 AMeV, as shown in Fig. 5(c). A Fourier analysis of density fluctuations cannot be readily applied to open systems. Thus, in order to extract the fluctuation growth rate, we adopted a numerical procedure based on the recognition of cluster correlations and associated chronology. More precisely, we estimated the breakup time of the jet, t_{split}, as the average separation time of the clusters emerging from the jet, calculated since inhomogeneities start to arise. Then the growth rate is evaluated as $\Gamma_k = \hbar/t_{split}$. Such approach, introduced in ref. [25], estimates Γ_k satisfactorily in realistic physical conditions, at the price of some possible underestimation. In configurations where clusters are regularly aligned along the jet, we assume that the wavelength of the instability simply corresponds to the average spacing of two close clusters contained in the jet, see circles in Fig. 5(c). On the other hand, when too many almost equal-size clusters make up the jet in a disordered pattern, in a sort of turbulent regime, the wavelengths are extracted from the average size d of the emerging clusters, as $\lambda = d \approx [6\langle A\rangle/(\pi\rho)]^{1/3}$, see squares in Fig. 5(c). We find that the dispersion relation obtained from the jet fragmentation is clearly outside the surface instability region, favouring volume instabilities. Even though it is rather similar to the BLOB result in nuclear matter at $\rho_{sat}/3$ (compare full points and open diamonds), some remarkable anomalies appear. The combination of many densities (with $\Gamma_{k,vol}$ decreasing for larger ρ) shifts the maximum towards smaller wavelengths (larger k). Moreover, a backbending appears for small k modes, indicating the coexistence of volume and surface instabilities, with larger wavelengths resulting from a combination between the two effects. We confirm that, as expected from the study reported in Fig. 3(b), the formation of clusters which abound in the jet, and which correspond to large k is essentially due to a combination of dissipation and fluctuations in the bulk, exhibiting a granular-like behaviour. Indeed, for large k values, the growth rates associated with the jet fragmentation are rather close to the results related to volume instabilities (compare full squares and open diamonds in Fig.5). To some extent, the jet fragmentation features discussed here may recall, because of the dynamical origin of the jet fragments, the observation of nucleons populating the high-energy tails of the spectra measured in nuclear reactions, the so-called Fermi jets [43, 44]. However, while the latter mechanism is interpreted in an individual-nucleon picture, the jet fragments discussed therein correspond to the development of collective mean-field (surface or volume) instabilities. In reactions at Fermi energies, the resulting kinematics may display comparable features, corresponding to a smooth transition between the two processes.

5. Conclusions

We undertook the modelling of nuclear jets in heavy-ion collisions in the Fermi-energy range, i.e. the appearing of collimated streams of low-density matter. At variance with other dissipative mechanisms in nuclear dynamics, the jet formation has not been explicitly addressed so far, even though it has been reported in experiments (see ref. [28]). We found that nuclear jets are described when collisional correlations and fluctuations in full one-body phase space are included, relying on a full solution of the Boltzmann-Langevin equation. In this case, we point out for the first time the concurrent role of volume and shape instabilities. Our calculations show that the disassembling of the jet occurs mainly by a combination of volume instabilities over a range of densities which extends below 1/4 of saturation density, rather than by Rayleigh surface instabilities. The mechanism favours the production of small fragments, down to light clusters. Only a residual surface contribution affects the largest wavelengths, indicating a possible transition from volume to surface instabilities. The vanishing contribution of cohesive forces in the clusterisation of the jet, inspires a suggestive analogy between nuclear jets and the development of packets in granular streams of dry sand which, in absence of surface tension, can break up into packets even in vacuum after some distance is travelled [55, 56, 57, 58, 59]. The jet mechanism and the associated collimated streams of clusters could be addressed experimentally with new detection systems measuring isotopic identification, angular correlations and cluster coincidences on a event-by-event basis. Not only this mechanism would be confirmed, but also non-equilibrium features like the dynamics of cluster formation and growth rates investigated in this work could be more directly accessed, opening novel frontiers. Reaction mechanisms sensitive to the interplay between surface and volume instabilities like nuclear jets can also shed light on relevant features of the nuclear effective interaction.

Acknowledgments

Research was conducted under the auspices of the International Associated Laboratory (LIA) COLL-AGAIN. Funding from the European Union's Horizon 2020 research and innovation program under Grant No. 654002 is acknowledged.

Appendix A. Simulation and analysis details

The Boltzmann-Langevin (BL) treatment of Eq. (1) as well as applications to instabilities and fluctuating behaviours are described in details in ref. [25]. Through a Wigner transform, some correspondence can be established with the stochastic TDHF [17, 45] scheme. The reduced one-body phase-space density f^n in Eq. (1) replaces in fact the Slater representation in

the TDHF approach and corresponds to Fermi statistics at equilibrium. The residual contributions are replaced by modified Uehling-Uhlenbeck (UU) terms, where each single in-medium collision event acts on extended equal-isospin one-body phase-space portions, large enough so that the occupancy variance in h^3 cells corresponds to the one associated with the scattering of two nucleons; this variance should equal $f(1-f)$ at equilibrium, in order to strictly avoid any violation of Pauli blocking at each single scattering event [46]. A solution of the BL equation was obtained in full one-body phase space, resulting in the following set of BLOB equations [24, 25]:

$$\frac{\partial f^{(n)}}{\partial t} - \{h^{(n)}, f^{(n)}\} = I^{(n)}_{\rm UU} + \delta I^{(n)}_{\rm UU} = \\ = g \int \frac{\mathrm{d}\mathbf{p}_b}{h^3} \int W_{(\rm AB\leftrightarrow CD)}\, F_{(\rm AB\rightarrow CD)}\, \mathrm{d}\Omega\,, \qquad \text{(A.1)}$$

where g is the degeneracy factor, W is the transition rate in terms of relative velocity between the two colliding phase-space elements, and F handles the Pauli blocking of initial (A,B) and final (C,D) states over their full one-body phase-space extensions.

All simulations presented in this study use a simplified SKM* effective interaction [47, 33] with incompressibility modulus $k = 200$ MeV and a linear parameterisations for the surface symmetry energy. $N_{\rm test} = 40$ test particles per nucleon are used to sample the mean field. A screened in-medium N-N cross section (from ref. [48]) is used. Starting from an initial configuration $t = 0$ where the projectile and target centres are spaced of 16 fm along the beam axis, the calculation is carried on until no new fragments appear and no further than 280 fm/c; it is then rewound back to the time of the last fragment separation $t_{\rm stop}$, which is different for each event. The secondary decay (analysed in Fig. 4) is calculated in flight while the system is driven by Coulomb propagation, using the transition state model Simon [49, 50].

The density dependence can be included in the surface tension γ in Eq. (2) as suggested in refs. [51, 52], so that

$$\frac{\gamma(\rho,\beta,T)}{\gamma_{\rm sat}} \approx F_T\left[1 - c_{\rm sym}\beta^2 - \chi\left(1-\frac{\rho}{\rho_{\rm sat}}\right)\right], \qquad \text{(A.2)}$$

where, according to the SKM* interaction, $\gamma_{\rm sat} = \gamma(\rho_{\rm sat}, \beta = 0, T = 0) \approx 1$ MeV fm^{-2}, $\rho_{\rm sat} \approx 0.16$ fm^{-3}, $c_{\rm sym} \approx 1.9$ and $\chi = (\rho_{\rm sat}/\gamma_{\rm sat})\partial_\rho\gamma|_{\rho_n=\rho_p=\rho_{\rm sat}/2} \approx 1.16$. F_T further introduces a temperature correction which, according to the proposal of ref. [53], imposes that the surface tension should vanish at the critical temperature of the nuclear liquid-gas phase transition ($T_{\rm c}$ ~18 to 20 MeV). In the conditions of the present study, corresponding to a temperature of about 3 MeV, the correction is still negligible, so that $F_T \approx 1$. Diffuseness and viscosity [54], which have counteracting contributions [8], as well as geometric distortion are neglected.

In Eq. (3), the ultraviolet cutoff is determined by the range of the nuclear interaction through a term related to surface tension and diffuseness. It consists of a Gaussian smearing $g(k)$ with a width of around 0.8 to 0.9 fm [25].

References

[1] J. Eggers and E. Villermaux, Physics of liquid jets, Rep. Prog. Phys. 71 (2008) 036601.
[2] M.C. Cross and P.C. Hohenberg, Pattern formation outside of equilibrium, Rev. Mod. Phys. 65 (1993) 851.
[3] A.C. Scott, The Nonlinear Universe: Chaos, Emergence, Life, Springer-Verlag, Berlin Heidelberg (2007).
[4] R. Vandenbosch and J.R. Huizenga, Nuclear Fission, Academic Press, New York and London(1973).
[5] J.J. Griffin and Kit-Keung Kan, Colliding heavy ions: Nuclei as dynamical fluids, Rev. Mod. Phys. 48 (1976) 467.
[6] J. Blocki, Y. Boneh, J.R. Nix, J. Randrup, M. Robel, A.J. Sierk, and W.J. Swiatecki, One-Body Dissipation and the Super-Viscidity, Ann. Phys. 113 (1978) 330.
[7] J.W.S. Rayleigh, Further observations upon liquid jets, in continuation of those recorded in the royal society's 'proceedings' for March and May, 1879, Proc. of the Royal Society XXXIV (1882) 130.
[8] U. Brosa, S. Grossmann, and A. Müller, Nuclear scission, Phys. Rep. 197 (1990) 167.
[9] N. Gopan and S.P. Sathian, Rayleigh instability at small length scales, Phys. Rev. E 90 (2014) 033001.
[10] C.P. Montoya, W.G. Lynch, D.R. Bowman, G.F. Peaslee, N. Carlin, R.T. de Souza, C. K. Gelbke, W.G. Gong, Y.D. Kim, M.A. Lisa, L. Phair, M.B. Tsang, J.B. Webster, C. Williams, N. Colonna, K. Hanold, M. A. McMahan, G.J. Wozniak, and L.G. Moretto, Fragmentation of Necklike Structures, Phys. Rev. Lett. 73 (1994) 3070.
[11] J. Tõke et al., Phys. Rev. Lett. 75 (1995) 2920.
[12] J.F. Lecolley et al., Neck formation and decay in Pb + Au collisions at 29 MeV/u Phys. Lett. B 354 (1995) 202.
[13] M. Di Toro, A. Olmi and R. Roy, Neck dynamics, Eur. Phys. J. A 30 (2006) 65.
[14] V. Baran, M. Colonna, V. Greco, and M. Di Toro, From multifragmentation to neck fragmentation: Mass, isospin, and velocity correlations, Phys. Rep. 410 (2012) 335.
[15] D. Lacroix and S. Ayik, Stochastic quantum dynamics beyond mean field, Eur. Phys. J. A 50 (2014) 95.
[16] Ph. Chomaz, M. Colonna, A.Guarnera and J. Randrup, Brownian One-Body Dynamics in Nuclei, Phys. Rev. Lett. 73 (1994) 3512.
[17] S. Ayik and C. Grégoire, Fluctuations of single-particle density in nuclear collisions, Phys. Lett. B 212 (1988) 269.
[18] P.-G. Reinhard, and E. Suraud, Stochastic TDHF and the Boltzman-Langevin Equation, Ann. of Physics 216 (1992) 98.
[19] D. Pines and P. Nozieres, The Theory of Quantum Liquids, Benjamin, New York (1966).
[20] S. Ayik, M.Colonna, and P. Chomaz, Quantal effects on growth of instabilities in nuclear matter, Phys. Lett. B 353 (1995) 417.
[21] Ph. Chomaz, M. Colonna, and J. Randrup, Nuclear spinodal fragmentation, Phys. Rep. 389 (2004) 263.
[22] B. Borderie et al. (INDRA collaboration), Phase transition dynamics for hot nuclei, Phys. Lett B 782 (2018) 291.
[23] M. Colonna, V. Baran, M. Di Toro, and H.H. Wolter Isospin distillation with radial flow: A test of the nuclear symmetry energy, Phys. Rev. C 78 (2008) 064618.
[24] P. Napolitani and M. Colonna, Bifurcations in Boltzmann-Langevin One Body dynamics for fermionic systems, Phys. Lett. B 726 (2013) 382.
[25] P. Napolitani and M. Colonna, Inhomogeneity growth in two-component fermionic systems, Phys. Rev. C 96 (2017) 054609.
[26] A. Guarnera, Ph. Chomaz, M. Colonna, and J. Randrup, Multifragmentation with Brownian one-body dynamics, Phys. Lett. B 403 (1997) 191.
[27] M. Colonna, M. Di Toro, A. Guarnera, S. Maccarone, M. Zielinska-Pfabé, and H.H. Wolter, Fluctuations and dynamical instabilities in heavy-ion reactions, Nucl. Phys. A642 (1998) 449.
[28] P. Lautesse et al. (INDRA collaboration), Evolution of the fusion cross-section for light systems at intermediate energies, Eur. Phys. J. A27 (2006) 349. See fig.4, and further preliminary analysis in L. Francalanza for INDRA collaboration, In medium fragment break-up of projectile in ^{58}Ar+^{36}Ni central collisions, J. Phys.: Conf. Ser. 863 (2017) 012061.
[29] Dynamics and Thermodynamics with Nuclear Degrees of Freedom, Eur. Phys. J. A 30 (2006) III.
[30] M. Colonna, P. Napolitani, and V.Baran, Mean-field instabilities and cluster formation in nuclear reactions, in "Nuclear Particle Corre-

lations and Cluster Physics", pp. 403-424, World Scientific (2017), arXiv:1604.03866.
[31] Lukasik et al. (INDRA collaboration), Dynamical effects and intermediate mass fragment production in peripheral and semicentral collisions of Xe+Sn at 50 MeV/nucleon, Phys. Rev. C 55 (1997) 1906.
[32] J. Colin et al. (INDRA collaboration), Dynamical effects in multifragmentation at intermediate energies, Phys. Rev. C 67 (2003) 064603.
[33] V. Baran, M. Colonna, M. Di Toro, and R. Zus, Reaction dynamics with exotic nuclei, Phys. Rev. c 85 (2005) 054611.
[34] M. Colonna and M.B. Tsang, Isotopic compositions and scalings, Eur. Phys. J. A30 (2006) 165.
[35] D.D.S. Coupland, W.G. Lynch, M.B. Tsang, P. Danielewicz and Y. Zhang, Influence of transport variables on isospin transport ratios, Phys. Rev C 84 (2011) 054603.
[36] Topical issue on Nuclear Symmetry Energy, Eur. Phys. J. A 50 (2014) 9.
[37] R. Lionti, V. Baran , M. Colonna, and M. Di Toro, IMF isotopic properties in semi-peripheral collisions at Fermi energies, Phys. Lett. B 625 (2005) 33.
[38] M. Di Toro, S.J. Yennello and B.-A. Li, Isospin flows, Eur. Phys. J. A 30 (2006) 153.
[39] C. Ducoin, Ph. Chomaz, and F. Gulminelli, Isospin fractionation: equilibrium versus spinodal decomposition, Nucl. Phys. A781 (2007) 407.
[40] M. Colonna, Ph. Chomaz, and A. Guarnera, Study of multifragmentation patterns induced by spinodal instabilities, Nucl. Phys. A613 (1997) 165.
[41] M. Colonna, Ph. Chomaz, and J. Randrup, Linear response in stochastic mean-field theories and the onset of instabilities, Nucl. Phys. A567 (1994) 637.
[42] M. Colonna and Ph. Chomaz, Unstable infinite nuclear matter in stochastic mean field approach, Phys. Rev C 49 (1994) 1908.
[43] J.P. Bondorf, J.N. De, G. Fái, A.O.T. Karvinen, B. Jakobsson, and J. Randrup, Promptly emitted particles in nuclear collisions, Nucl. Phys. A333 (1980) 285.
[44] K. Möhring, W.J. Świątecki, and M. Zielińska-Pfabè, Simple estimates for Fermi jets, Nucl. Phys. A440 (1985) 89.
[45] L. Lacombe, E. Suraud, P.-G. Reinhard, and P.M. Dinh, Stochastic TDHF in an exactly solvable model, Ann. Phys.(NY) 373 (2016) 216.
[46] J. Rizzo, Ph. Chomaz, and M. Colonna, A new approach to solve the Boltzmann-Langevin equation for fermionic systems, Nucl. Phys. A806 (2008) 40.
[47] A.Guarnera, M.Colonna, and Ph.Chomaz, 3D stochastic mean-field simulations of the spinodal fragmentation of dilute nuclei, Phys. Lett. B 373 (1996) 267.
[48] P.Danielewicz, Acta Phys.Polon. B33 (2002) 45; D.D.S. Coupland, W.G. Lynch, M.B. Tsang, P. Danielewicz and Y. Zhang, Phys. Rev. C 84 (2011) 054603.
[49] D. Durand, An event generator for the study of nuclear collisions in the Fermi energy domain (I). Formalism and first applications, Nucl. Phys. A541 (1992) 266.
[50] P. Napolitani and M. Colonna, Frustrated fragmentation and reaggregation in nuclei: a non-equilibrium description in spallation, Phys. Rev. C 92 (2015) 034607.
[51] K. Iida and K. Oyamatsu, Surface tension in a compressible liquid-drop model: Effects on nuclear density and neutron skin thickness, Phys. Rev. C 69 (2004) 037301.
[52] W. Horiuchi, S. Ebata, and K. Iida, Neutron-skin thickness determines the surface tension of a compressible nuclear droplet, Phys. Rev. C 96 (2017) 035804.
[53] D.G. Ravenhall, C.J. Pethick, and J.M. Lattimer, Nuclear interface energy at finite temperatures, Nucl. Phys. A407 (1983) 571.
[54] M. Baldo and G.F. Burgio, Properties of the nuclear medium, Rep. Prog. Phys. 75 (2012) 026301.
[55] D. Lohse, R. Bergmann, R. Mikkelsen, C. Zeilstra, D. van der Meer, M. Versluis, Ko van der Weele, M. van der Hoef, and H. Kuipers, Impact on Soft Sand: Void Collapse and Jet Formation, Phys. Rev. Lett 93 (2004) 198003.
[56] D. Lohse, R. Rauhé, R. Bergmann, and D. van der Meer, Creating a dry variety of quicksand, Nature brief comm. 432 (2004) 689.
[57] J.R. Royer, E.I. Corwin, A Flior, M.-L. Cordero, M.L. Rivers, P.J. Eng, and H.M. Jaeger, Formation of granular jets observed by high-speed X-ray radiography, Nature Phys. 1 (2005) 164.
[58] J.R. Royer, E.I. Corwin, B. Conyers, A. Flior, M.L. Rivers, P.J. Eng, and H.M. Jaeger, Birth and growth of a granular jet, Phys. Rev. E 78 (2008) 011305.
[59] J.R. Royer, D.J. Evans, L.Oyarte, Q.Guo, E.Kapit, M.E. Möbius, S.R. Waitukaitis, and H.M. Jaeger, High-speed tracking of rupture and clustering in freely falling granular streams Nature Lett. 459 (2009) 1110.